ACS SENSORS

Article

Cite This: ACS Sens. XXXX, XXX, XXX−XXX

pubs.acs.org/acssensors

Scalable Nanogap Sensors for Non-Redox Enzyme Assays

Xing Su,* Noureddine Tayebi,# Grace M. Credo,# Kai Wu,# Oguz H. Elibol,# David J. Liu,† Jonathan S. Daniels,‡ Handong Li,§ Drew A. Hall,∥ and Madoo Varma⊥

Intel Labs, Intel Corporation, 2200 Mission College Boulevard, Santa Clara, California 95054, United States

Supporting Information

ABSTRACT: Clinical diagnostic assays that monitor redox enzyme activity are widely used in small, low-cost readout devices for point-of-care monitoring (e.g., a glucometer); however, monitoring non-redox enzymes in real-time using compact electronic devices remains a challenge. We address this problem by using a highly scalable nanogap sensor array to observe electrochemical signals generated by a model non-redox enzyme system, the DNA polymerase-catalyzed incorporation of four modified, redox-tagged nucleotides. Using deoxynucleoside triphosphates (dNTPs) tagged with *para*-aminophenyl monophosphate (pAPP) to form pAP-deoxyribonucleoside tetra-phosphates (AP-dN4Ps), incorporation of the nucleotide analogs by DNA polymerase results in the release of redox inactive pAP-triphosphates ($pAPP_3$) that are converted to redox active small molecules *para*-aminophenol (pAP) in the presence of phosphatase. In this work, cyclic enzymatic reactions that generated many copies of pAP at each base incorporation site of a DNA template in combination with the highly confined nature of the planar nanogap transducers (z = 50 nm) produced electrochemical signals that were amplified up to 100,000×. We observed that the maximum signal level and amplification level were dependent on a combination of factors including the base structure of the incorporated nucleotide analogs, nanogap electrode materials, and electrode surface coating. In addition, electrochemical signal amplification by redox cycling in the nanogap is independent of the in-plane geometry of the transducer, thus allowing the nanogap sensors to be highly scalable. Finally, when the DNA template concentration was constrained, the DNA polymerase assay exhibited different zero-order reaction kinetics for each type of base incorporation reaction, resolving the closely related nucleotide analogs.

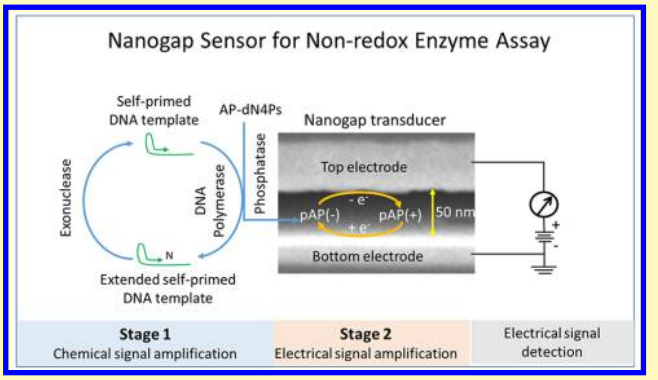

KEYWORDS: *nanogap sensor, redox-cycling, electrochemical assay, non-redox enzyme, enzyme kinetics, DNA polymerase, pyrophosphate*

Enzymes are catalysts of biochemical reactions within living organisms involved in a variety of processes such as DNA replication, protein synthesis, and sugar metabolism. Common approaches for assaying enzyme activity include monitoring substrates and/or products using colorimetric or fluorimetric techniques, radioactive detection methods, liquid chromatography, and mass spectrometry.[1] Many of these techniques are not amenable to high throughput and/or automation and they are not intended for portability and ease-of-use. With the advancement of microelectronics, the activity of some enzyme−substrate systems that are redox active can now be readily measured electrically with cost-effective and compact electrochemical devices,[1,2] such as a glucometer; however, monitoring non-redox enzyme reactions remains limited to bulky[3] and/or costly optical[4] instruments. For example, the use of fluorogenic substrates is the gold standard for continuously monitoring assays of tyrosine and serine phosphatases, which are of interest for drug discovery.[1] Fluorescence-based assays for other enzymes found in blood are widely used in clinical diagnoses of lysosymal storage diseases (LSD's) such as Tay-Sachs and Gaucher using commercially available, synthetic coumarin 4-methylumbelliferone (4-MU).[5]

Direct and reliable approaches to the electrical assay of non-redox enzymes would necessitate mechanisms that would allow for stable electrical signal generation from reactions involving non-redox enzymes, such as the DNA polymerase for deoxyribonucleotide triphosphate (dNTP) incorporation. Non-redox enzymes such as DNA polymerase, RNA polymerase, aminoacyl-tRNA synthetase (for protein synthesis), and UDP-Glucose pyrophosphorylase (for glycogen synthesis) are all essential to living organisms.[6] One common feature of these enzymes is that they release inorganic pyrophosphate (PPi) as one of their reaction byproducts.[7−9] In order to test the feasibility of performing electrical kinetic assays of such non-redox enzymes, we targeted the PPi-releasing chemistry of DNA polymerase and related enzymes by designing a set of four dNTP analogs as reaction substrates with a redox mediator (*para*-aminophenol or pAP) attached through the polyphosphate linkage (pAP-deoxyribonucleoside tetra-phos-

Received: June 16, 2018
Accepted: August 29, 2018
Published: August 29, 2018

DOI: 10.1021/acssensors.8b00500
ACS Sens. XXXX, XXX, XXX−XXX

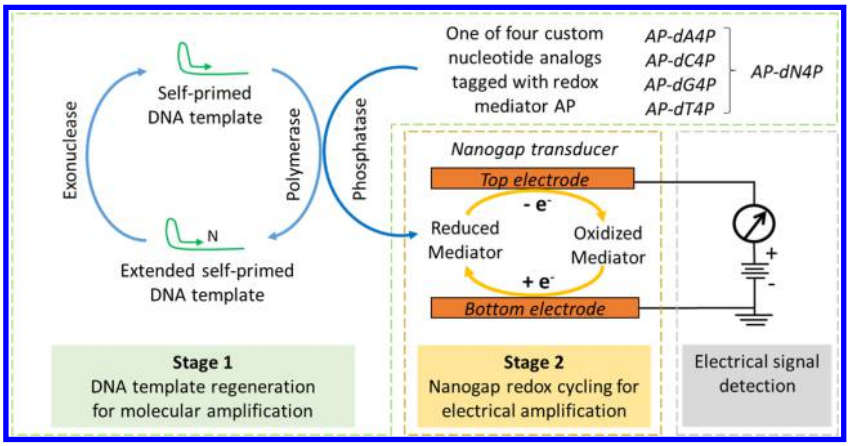

Figure 1. Scalable nanogap-based sensing system for observing non-redox enzyme reactions, including signal generation, amplification, and transduction. Stage 1 is a self-primed DNA template regeneration process using extended self-primed DNA template molecules, which involves the cleavage of monophosphate nucleotides by the exonuclease, reincorporation of one of the four redox-modified nucleotide analogs (AP-dN4Ps) by the polymerase, and release of reaction products ($pAPP_3$) that are converted to redox-active molecules (pAP) in the presence of phosphatase. Stage 2 is an electrical signal amplification and transduction process, in which pAP molecules in solution undergo redox cycling in a planar electrode gap device. The collectively amplified electrical signal can be detected in real-time by an external electronic device.

phates or AP-dN4Ps). We hypothesized that production rates of pAP could be used to assess the properties of both the non-redox enzymes and their substrates.

To measure electrical signals of pAP efficiently, we developed a biochemical sensing system that enables molecular amplification, electrochemical signal generation, and amplified electrical signal detection on a scalable nanogap sensor chip (Figure 1). In this sensing system, non-redox DNA polymerase utilizes AP-dN4P nucleotide analog substrates in cyclic enzymatic reactions to release redox inactive pAP-triphosphates ($pAPP_3$). After the released $pAPP_3$ molecules react with phosphatase, the resulting redox-active pAP molecules undergo redox cycling in a nanogap device to transduce and amplify the biochemical signals (in the form of molecules at certain concentrations) to electrical signals (in the form of currents or potentials). We use the term redox-genic to refer to the property of redox-inactive molecules that can be converted to redox-active molecules. With this sensing system, we demonstrate the ability to differentiate structurally similar nucleotide analogs electrically and kinetically. Our findings suggest that the principle of our sensing system can potentially be used for nucleotide analog drug screening and nucleic acid sequence analysis, and could also be applied to assaying other pyrophosphate (PPi)-releasing non-redox enzymes.

We have previously reported chemically modified field-effect transistor (FET)-based silicon nanoplate devices to directly detect DNA polymerase reaction product PPi from DNA incorporation reactions,[10,11] but due to unfavorable signal-to-noise ratio (SNR) issues as the active sensing area is reduced, these devices were not amenable to further scaling down to the targeted 1 μm^2 pixel sizes. In contrast to FET-based devices, the electrical SNR in redox cycling of redox molecules in a nanogap transducer device is independent of the in-plane geometry of the transducer thus allowing the transducers to be highly scalable (with constant signal-to-noise ratio).[12] The employment of nanogap sensors not only enables the scaling of the sensor devices but also eliminates the need for analyte-specific surface modification and, furthermore, permits real-time measurement of concentration changes of reaction products, which is critical to enzyme kinetic assays. This type of nanogap sensor can be reliably fabricated in a CMOS (complementary metal oxide semiconductor) compatible manner, which facilitates dense integration of sensor units (and associated electronics) onto a single platform, such as a silicon chip typically used in integrated circuit manufacturing applications.[12]

RESULTS AND DISCUSSION

In this work, cyclic enzymatic reactions that generated many copies of redox-active small molecule para-aminophenol (pAP) from each base incorporation site of a DNA template in combination with the highly confined nature of the planar nanogap transducers (z = 50 nm) produced electrochemical signals that were amplified up to 100,000×. As shown in Figure 1, Stage 1 is a self-primed DNA template regeneration process using extended self-primed DNA template molecules with nuclease-resistant priming ends in cyclic non-redox enzymatic reactions, which involve the cleavage of monophosphate nucleotides by the exonuclease and reincorporation of one of the four redox-modified nucleotide analogs (AP-dN4Ps) by the polymerase. This reaction releases $pAPP_3$ molecules as reaction products that are converted to redox-active pAP molecules in the presence of phosphatase. This reaction cycle results in chemical amplification of pAP for a specific site in a DNA template (20× to 200× in 10 min; Figure S1). Stage 2 is an electrical signal amplification and transduction process, in which pAP molecules undergo redox cycling for electrochemical signal amplification in a planar electrode gap (nanogap). The redox cycling transduces the pAP chemical concentration to an amplified electrical signal (100× to 500× in 10 min).[12,13] The collectively amplified electrical signal (as much as 100,000×), which is linearly proportional to the input DNA template concentration, can be detected in real-time by an external electronic device.

Planar nanogap devices were designed and fabricated for this work because they can transduce biochemical information to electrical information directly and hence amplify the signal significantly via redox cycling when the electrode gaps are 300 nm or less.[12−14] Since the sensitivity and redox cycling ability of these sensors depend only on the gap between bottom and top electrodes, they are easily amenable to down-scaling sensor

DOI: 10.1021/acssensors.8b00500
ACS Sens. XXXX, XXX, XXX−XXX

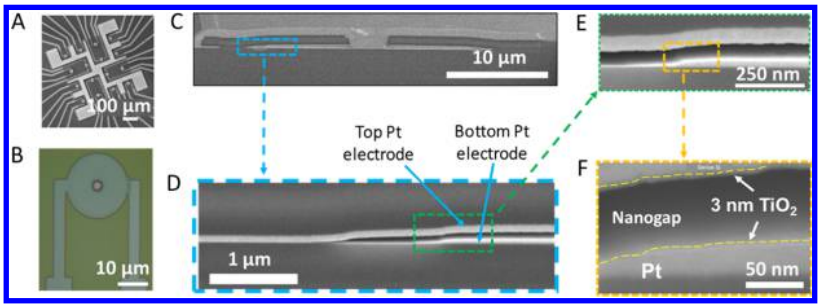

Figure 2. Nanogap transducer characterization. (A) Optical microscopy image of the fabricated 4 × 4 nanogap sensor array showing a common reference electrode (a large, connected metal plate) and electrical connects to the nanogap devices. (B) Optical microscopy image of a single nanogap transducer pixel (d = 20 μm). (C) Cross-sectional scanning electron microscopy image (XSEM) of the transducer. (D) XSEM image from the boxed area of C showing a closer view of the edge of the nanogap formed by the two Pt electrodes. (E) XSEM from the boxed area of D showing the nanogap (~50 nm) between the two Pt electrodes. (F) XSEM from boxed area of E showing the nanogap with TiO_2 (~3 nm) coating on the top and bottom Pt electrodes.

pixel size in the x and y dimensions while maintaining the SNR observed in larger devices.[14,15]

In a nanogap device, signal strength, represented by current I, is limited by diffusion rate D (the diffusivity) or is inversely proportional to the time it takes for trapped redox-active molecules N to diffuse between the two electrodes:

$$I = NeD/z^2$$

where e is the elemental charge and z is the vertical (out-of-plane) spacing between the two electrodes. For a given concentration of a redox molecular species, N is proportional to the surface area (a) of the nanogap device with a given z. Thus, when signal and noise from a nanogap device alone are considered and electrical noise from the instrumentation is not dominant, shrinking the electrode surface dimensions generates a smaller output current, but at the same time the double-layer capacitance associated with the electrochemically active electrodes is also reduced. This suggests that nanogap transducer sensitivity, which is mainly determined by SNR, is independent of the nanogap surface area, a. It has been shown that these type of nanogap devices can detect redox compounds at the single molecule level.[16]

In this study, we created a 4 × 4 array of circular nanogap transducers (d = 20 μm, z = 50 nm, V = 16 fL, see Figure 2A and B). Each of the nanogap devices had an access hole at the center for uniform sample distribution by capillary action and diffusion.[12] Each transducer device consisted of two planar platinum (Pt) electrodes (Figure 2C,D,E; Figure S2). In addition to Pt, we have also used other electrochemically inert materials, such as gold (Au)[12] and conductive ultrananocrystalline diamond,[17] as paired nanogap electrodes, as well as asymmetric nanogap structures fabricated with different materials for top and bottom electrodes. Although Au is more inert and has better electrochemical properties than Pt, Au is known to have interdiffusion issues[17] at relatively low processing temperatures (<200 °C) and the nanocrystalline diamond process requires an annealing step with temperature of >800 °C that is too high to be compatible with the thermal budget of standard process technologies for semiconductor fabrication and monolithic CMOS integration.[17−19] With the eventual goal of scaling the device manufacturing process for standard semiconductor fabrication, we proceeded with Pt nanogap electrodes. As shown in Figure 2B, the devices used for these experiments were 20-μm-diameter nanogap transducers with overlapping top and bottom electrode areas of ~300 μm^2. In order to demonstrate scaling and facilitate integration with underlying integrated circuits, we have also designed and fabricated arrays of smaller nanogap transducers, such as 4 × 5 μm^2 pixels[20] and 1 × 1 μm^2 pixels (Figure S3).

para-Aminophenol (pAP or AP) was selected as the mediator in the assay system because it is redox-active and can be produced from redox-genic pAP-phosphates ($pAPP_n$, n = 1 for monophosphate, n > 1 for polyphosphates) after dephosphorylation[21] (Figure 3) by phosphatase. However, we

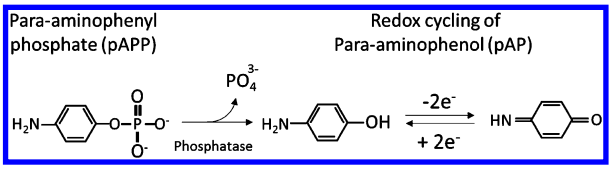

Figure 3. Chemical reactions illustrating the conversion of redox-genic pAPP to redox-active pAP and subsequent redox cycling of pAP.

noticed that the redox cycling signal from pAP in a Pt nanogap device could drop by as much as 50% after 100 cyclic voltammetry (CV) scans (Figure 4A). We traced the primary source of the signal decrease to Pt-catalyzed pAP degradation. In bulk electrode (non-nanogap) studies, we observed that the initial current level of the pAP signal was degraded when pAP solutions were exposed to a nonscanning Pt electrode surface while pAP solutions exposed to gold- or diamond-based electrodes maintained their original electrochemical and optical absorbance properties (Figure S4). Based on these observations, Pt electrodes appeared to catalyze the conversion of pAP molecules in solution to benzoquinone (BQ), hydroquinone (HQ), and quinhydrone (QH) (Figure S5), which were identified by comparing the used solutions (scanned or not scanned but exposed to Pt, Au, or diamond) to solution standards of pAP, BQ, and HQ. In contrast, we observed that the Pt catalytic degradation effect could be greatly reduced when the Pt electrode surfaces were passivated (Figure S6). This suggests that the adverse catalytic effect of Pt could be mitigated by preventing pAP from direct contact with Pt electrodes through a surface coating, which, in turn, could deter electrode fouling due to deposition of polymerized products resulting from pAP degradation.

To achieve robust redox cycling results, we passivated the Pt electrode surfaces with a 3 nm TiO_2 dielectric film (Figure 2E and F). TiO_2 was chosen because its conduction band position is close to the Pt work function, which enables electron tunneling or hopping through the low energy barrier to

DOI: 10.1021/acssensors.8b00500
ACS Sens. XXXX, XXX, XXX−XXX

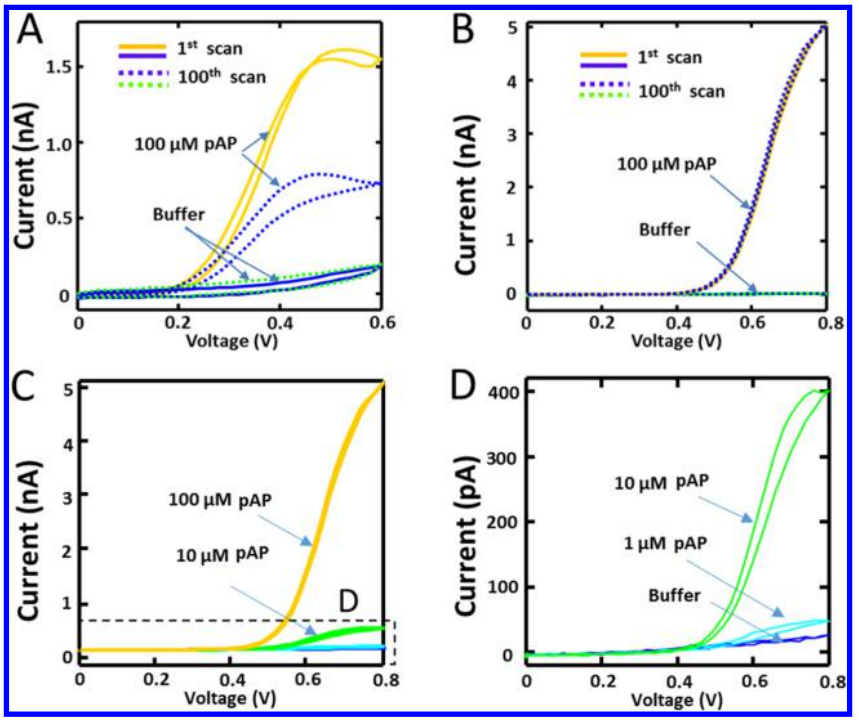

Figure 4. Electrochemical measurements of pAP standard solutions in nanogap sensors with bare Pt or coated Pt electrodes. (A) Cyclic voltammograms (CVs) of pAP from the first and 100th scans compared to a buffer solution on an uncoated nanogap device showing degradation of the current. For redox cycling of pAP, the potential at the bottom electrode was scanned from 0 to 0.7 V while the top electrode potential was kept constant at 0 V. (B) CVs of pAP from the first and 100th scans compared to a buffer solution on a TiO_2-on-Pt coated nanogap device, exhibiting stable current level over 100 cycles. (C) CVs of pAP as a function of concentration (0 to 100 μM) on a TiO_2-coated nanogap device. (D) Portion of C, showing CVs of lower concentrations of pAP from 0 to 10 μM.

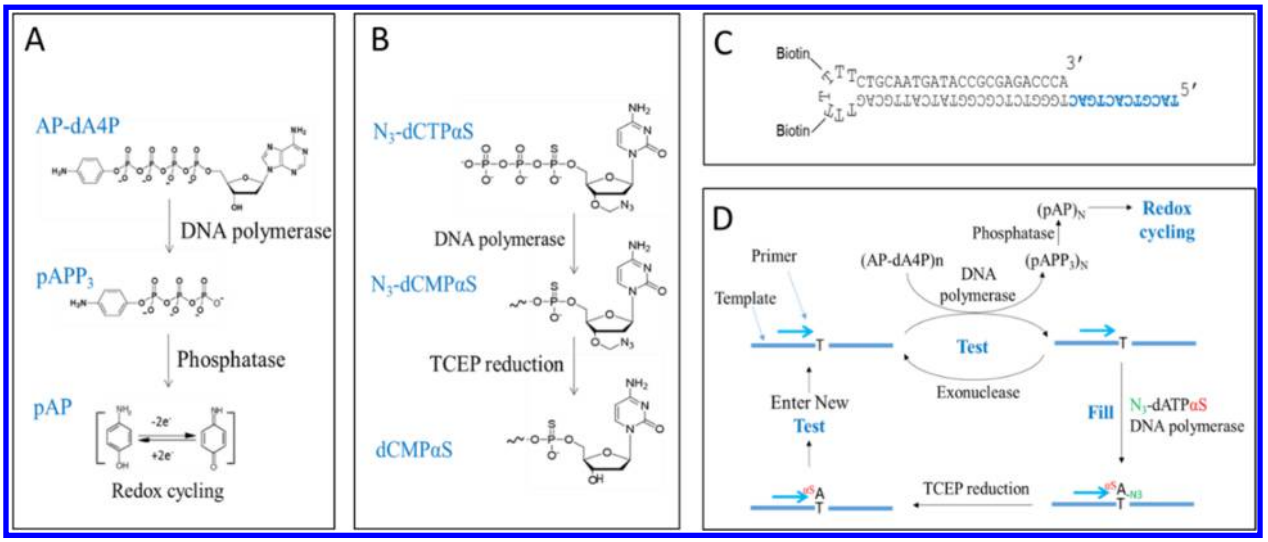

Figure 5. Molecular structures of synthesized nucleotide analogs and their functional roles in the TEST & FILL reaction scheme introduced in Figure 1 (Stage 1 chemical amplification). (A) Structures of aminophenol-deoxyribonucleoside tetra-phosphates (only AP-dA4P shown) and generation of $pAPP_3$ and pAP. (B) Structures of bifunctional nucleotide analogs (3′-*O*-azidomethyl α-thiol-dNTPs or N_3-dNTPαS, only N_3-dCTPαS shown); TCEP (tris(2-carboxyethyl)-phosphine) is a reducing agent used to remove the 3′-*O*-azidomethyl group. (C) Sequence and structure of the self-primed DNA template used in the current study. (D) Reaction scheme of TEST reaction (cyclic reactions of polymerase and exonuclease) at one base position for template regeneration and production of amplified pAP molecules, and FILL reaction (incorporation of exonuclease resistant bifunctional nucleotide) enabling next set of TEST reactions at the next base position.

maintain a similar electron transfer rate as with bare electrodes.[22] Figure 4B shows that the CV curves were not affected after extensive redox cycling and the current could be 3× higher from coated devices than uncoated devices. It is apparent that the inflection points of the CV curves from the coated nanogap devices were about 0.3 V higher than noncoated devices (Figure 4A and B). This was anticipated because electron transfer during redox cycling had to overcome the additional energy barrier formed between the TiO_2 conduction band and the Pt work function which necessitated a shift in the scanning voltage range. We also observed that the use of higher voltages reduced the reversibility of cyclic

DOI: 10.1021/acssensors.8b00500
ACS Sens. XXXX, XXX, XXX−XXX

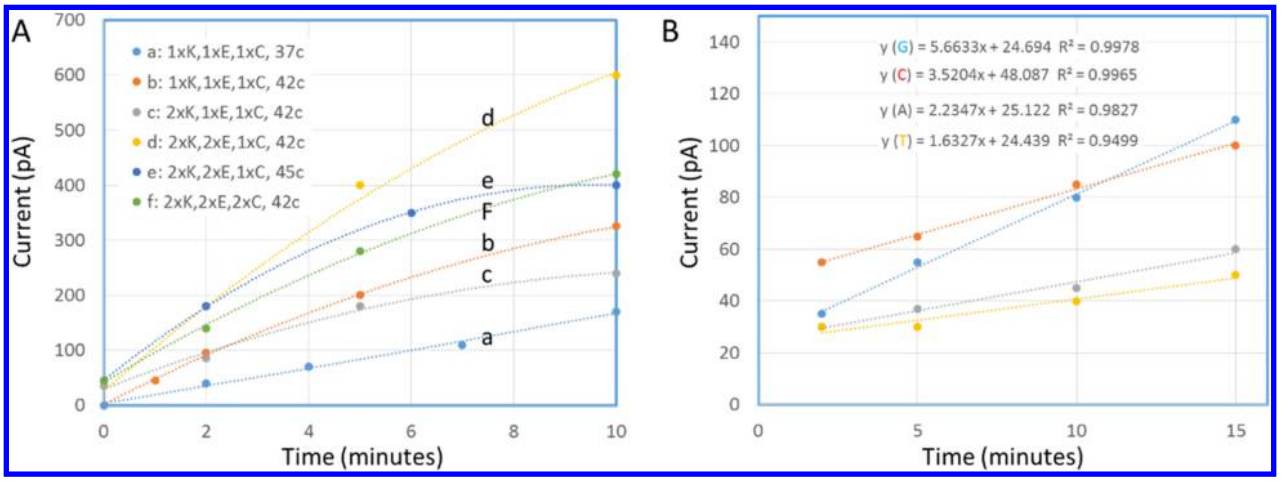

Figure 6. Resolving different reaction rates from the nucleotide analogs. The reactions were performed on the surface of a nanogap array in a flow cell (on-chip reaction). (A) Reaction rates observed using different enzyme ratios and under different reaction temperatures. Letter E for exonuclease, K for Klenow fragment of DNA polymerase I, and C for calf intestine alkaline phosphatase. 2× indicates twice as much enzyme concentration as 1× (for details, see Experimental Section). The curves were obtained from polynomial fitting: $y = k_1x^2 + k_2x + c$, where y is the electrical current signal from a nanogap device and x is time in minutes; k_1, k_2, and c are constants; when $|k_2/k_1| > 50$, the reactions were considered zero order when $x < 10$ min. (B) Linearly fitted curves from TEST reactions of the 4 AP-dN4Ps for the last (sixth) site in the template sequence where the correct matching base T was called.

voltammograms, possibly due to formation of irreversible degradation products of pAP at higher potentials. For these reasons, we defined a scanning voltage based on the current onset of the CV curves instead of using a fixed scanning range.

Comparing Figure 4A and B, the baseline current from the plain buffer was significantly reduced on the coated devices. Less than 1 μM pAP ($<1 \times 10^4$ molecules inside the nanogap) was readily detected and the electrical responses were proportional to pAP concentrations (Figure 4C,D, and Figure S7). With a coated nanogap device, for a given pAP concentration in an aqueous buffer, we found that redox cycling (bias between the top and the bottom electrodes of a nanogap, relative to reference ground electrode) could generate as much as a 500-fold increase in current compared to non-redox cycling (bias on the bottom electrode only with the top electrode disconnected). The amplification power of redox cycling constitutes the Stage 2 amplification in the assay scheme (Figure 1).

To demonstrate that pAP could be the mediator in coupling nanogap transducers with a non-redox enzyme system, we designed and synthesized a complete set of four pAP-deoxyribonucleoside tetra-phosphates (AP-dN4Ps) (Figure 5A). Our preliminary experimental data showed that the tetra-phosphate chain was the best spacer for ensuring efficient incorporation by DNA polymerase when compared with tri-, penta-, and hexa-phosphate chains. Because a pAP moiety was covalently attached to the terminal phosphate of the tetra-phosphate chain of a nucleotide, the nucleotide analog was resistant to phosphatase degradation. When an AP-dN4P was incorporated to a DNA primer, $pAPP_3$ was released as a byproduct. Like pAPP,[21] the redox-genic $pAPP_3$ could be converted to the redox-active pAP *in situ* by phosphatase. Thus, the electrochemical signals from the generated pAP reaction products could facilitate electronic measurement of the enzymatic incorporation of the nucleotide analogs.

In fulfilling the requirements for the cyclic enzyme assay scheme (Figure 1 and Figure 5D) as well as more complex reactions to be discussed later, we also designed and synthesized a set of bifunctional nucleotides (3′-*O*-azidomethyl α-thiol-dNTPs or N_3-dNTPαS) (Figure 5B) and used them to render a self-primed test template nuclease-resistant[23] (Figure 5C). The 3′-*O*-azidomethyl group in the nucleotide analogs reversibly blocked the 3′-end so that no repetitive nucleotides could be polymerized in a polymerase reaction, which was crucial to characterizing a template sequence.[24]

Figure 5D shows the two cyclic enzyme reactions in our non-redox enzyme assay scheme: the TEST reaction and the FILL reaction. The TEST reaction is the Stage 1 amplification shown in Figure 1. It includes a DNA polymerase, an exonuclease, and a phosphatase. When a complementary nucleotide analog has been incorporated to the priming end of the DNA complex by the polymerase, a $pAPP_3$ would be released that in turn could be converted to pAP by the phosphatase for redox cycling. Once the DNA polymerase leaves the priming site,[25] the exonuclease cleaves only the newly incorporated nucleotide assuming the prior nucleotide is nuclease-resistant (see FILL reaction below), resulting in regeneration of the DNA template molecule for a new round of incorporation of the same nucleotide in the same site. This TEST reaction is like the previously reported idling reactions.[26] When we compared pAP production in test tube reactions at a given DNA template concentration, we found there could be 20−50× more pAP generation from AP-dT4P and AP-dA4P, and 100−200× more pAP generation from AP-C4P and AP-dG4P (Figure S1 and Figure S7).

The FILL reaction has been designed to advance the primer by a single base. To achieve this, a DNA polymerase reaction takes place in the presence of a set of bifunctional nucleotides (Figure 5B), and only one of the matched nucleotides is incorporated to the 3′-end of the primer that is annealed to the DNA template molecule. After removing the reversible terminator from the newly incorporated nucleotide analog, the primer−template complex is ready for another round of TEST reaction. The combination of the TEST and the FILL reactions that were used for mini-sequencing reaction tests are discussed in the following sections.

The TEST reaction governs the reaction kinetics that are characteristic to key components of the reaction system.

DOI: 10.1021/acssensors.8b00500
ACS Sens. XXXX, XXX, XXX−XXX

According to reaction rate laws,[27] a full mathematical model of the rate of pAP production in our assay system could be complex. However, our unique enzyme system made it possible to obtain an abridged kinetic model. Assuming the phosphatase reaction was not the rate limiting step because of high substrate affinity[28] and both exonuclease and polymerase activities were unchanged during reactions, we can treat the production rate (p) of $pAPP_3$ as the rate of pAP generation. Thus, we have

$$p = k[N][T]$$

where k is the rate constant for a given enzyme (enzyme-dependent constant), N is the concentration of a nucleotide analog, and T is the DNA template concentration. Because nucleotide analog substrates were provided in a great excess and the DNA template molecules were regenerated by the TEST reactions, thus pAP or $pAPP_3$ production rate can be approximated to be a zero-order reaction (see Supporting Information)

$$p = K$$

where K is a reaction-dependent constant.

This implies that the redox-active species production rate can be considered to be relatively constant, which reflects the properties of nucleotide analogs, the DNA templates, and enzymes, provided that their concentrations were unchanged (or remained relatively high) during the reactions. For example, for a given set of enzymes and a template sequence, different nucleotide analogs would be associated with different K values.

To corroborate the zero-order kinetics, we assembled reactions using a known amount of a self-primed DNA template and an excess amount of a nucleotide analog but changed the relative ratios of the enzymes. According to polynomial curve fitting, near linear responses of pAP productions were obtained when the ratio of exonuclease to polymerase was maintained at 1:1 or higher (Figure 6A and Table S1). This agrees with the assumption that template regeneration by exonuclease was critical to maintaining the DNA template at a constant concentration. It was also observed that increasing temperature accelerated initial reaction rates, but reactions approached plateau values more rapidly at 45 °C than at lower temperatures. This was not unexpected because the enzyme-dependent reaction rate constant k is a function of temperature and higher temperatures can increase the chance of enzyme denaturation, decreasing the concentration of active enzyme and potentially violating the conditions for a zero-order reaction.

According to zero-order reaction rate kinetics, it would be possible to identify complementary bases of a DNA template sequence simply based on analyzing the relative incorporation rates of different nucleotide analogs for the same template site (priming site). We tested this hypothesis by attempting short DNA sequencing (mini-sequencing) through consecutive TEST & FILL cycles in a flow cell chamber where the surface ($500 \times 500\ \mu m^2$) of a 4×4 nanogap transducer array with DNA template molecules attached was exposed (Figure S8). In the flow cell chamber (~400 nL), enzymatic reactions took place near the nanogap transducers so that the reaction products could be detected in real-time when TEST reactions were taking place. In 7 consecutive TEST & FILL cycles, 28 pAP generation rate measurements (after a total of 35 enzymatic reactions) showed linear responses over more than 15 min (Figure 6B). Based on the rates of TEST reactions for all 4 nucleotide analogs, we were able to correctly identify the first 5 bases complementary to the test template sequence. The efficiency of the on-chip system, with reactions occurring on the chip surface, can be improved when more extensive sequencing is desired. To demonstrate the robustness of the assay system and apply reaction rates to direct template characterization, we also performed consecutive TEST & FILL reactions with the same DNA template sequence in test tubes (off-chip system, with reactions in solution suspensions). After analyzing normalized reaction rates, we were able to identify 8 of the 9 bases tested correctly after over 50 reagent exchanges for enzymatic and chemical reactions (Figure 7). The fifth base

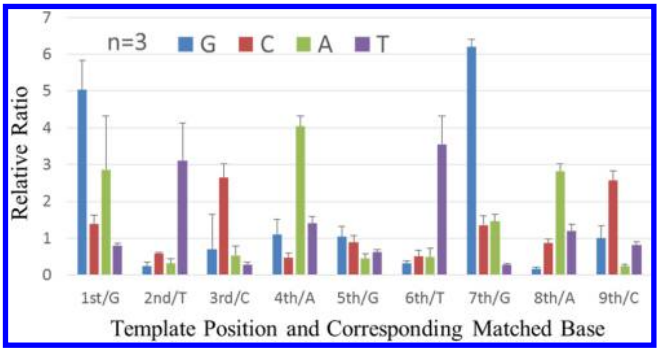

Figure 7. Mini-sequencing results of three replicated reactions. The relative ratios were calculated for each nucleotide analog per procedures described in the Experimental Section and Supporting Information. The highest ratio signal for each given site indicates the identity of the interrogated base.

was considered to be undetermined due to the insignificant difference between bases G and C. In the future, we would recommend optimizing reaction conditions to differentiate each nucleotide analog and increasing reaction redundancy, which is a procedure routinely implemented in current commercial sequencing solutions using other transduction mechanisms.

It is worth noting that, by comparing the rates of nucleotide analog incorporation, nucleotide analogs G and C had faster incorporation rates than nucleotide analogs A or T (Figure S9). This observation is consistent with previously mentioned rate differences in the incorporation of these nucleotide analogs to their corresponding complementary sites (correctly paired) and agrees with published information.[29] It was also observed that, under TEST conditions, the correctly paired nucleotide incorporation rates were typically within the range of 2−5× the rates of mispaired nucleotide analog incorporations (Figure 7). This agrees with the notion that achieving high fidelity of DNA polymerase reaction would require far more complex conditions than simple base-pairing.[30] Since these nucleotide analog structures are the same except for their bases, the incorporation rate differences suggest that the current electrochemical assay system should be able to differentiate other base modifications. Finally, at a given concentration of DNA template, we observed that the maximum signal level and amplification factor were dependent on a combination of factors including nucleotide structures, nanogap electrode materials, and electrode surface coating materials. Further optimization of these components in this sensing system has the potential to improve the assay results.

DOI: 10.1021/acssensors.8b00500
ACS Sens. XXXX, XXX, XXX−XXX

CONCLUSIONS

We have demonstrated a nanoscale electrochemical sensing system for the real-time and sensitive characterization of the PPi-releasing non-redox enzyme DNA polymerase as a function of different redox-tagged nucleotide analogs. In this system, the nanogap device serves as both a chemical–electrical transducer and an electrochemical signal amplifier. We have also shown that the non-redox enzyme reactions enable DNA template regeneration, which exhibits zero-order reaction kinetics and thus linear amplification of the redox-active mediator. The coupled two-stage amplification system can enhance signal up to 100,000× so that a signal equivalent to as few as 100 template molecules inside a nanogap device can be electrically measured. Since PPi or Pi release is widely present in the metabolic pathways of all living organisms, e.g., DNA and RNA synthesis, protein synthesis, and glycogen synthesis,[6,7] redox-active pAP can be a common mediator in electrochemical kinetic assays of related non-redox enzymes. We envision that this assay system can be used to facilitate the development of compact, electronic devices that can be used to determine the causes or states of metabolic disorders based on monitoring enzymatic activity,[31,32] identify genetic mutations or pathogens based on nucleic acid mini-sequencing,[33] or screen nucleotide analogs as potential candidates of antiviral or anticancer drugs.[34,35]

EXPERIMENTAL SECTION

Nanogap Transducer Design and Fabrication. The sensor array used in this study had identical and individually addressable nanogap transducers in 4 × 4 format, with each sensor having a diameter of 20 μm, corresponding to an electrode area of ~300 um^2. The chip dimension was 6 × 6 mm. Electrical contact pads were located along the 4 edges of the chip. The nanogap fabrication process used in this study is outlined in Figure S2.

Flowcell and Fluidic Control. For redox cycling measurements using nanogap devices in a 4 × 4 transducer array chip, a flow-cell was formed between the chip surface and a silver head, which were separated by a laser-cut gasket. To measure pAP generated from test tube reactions (off-chip reactions), a normal nanogap transducer array was used. For measurements of *in situ* generated pAP (on-chip reactions), a nanogap transducer array with physically immobilized magnetic beads functionalized with DNA template molecules was used (see Figure S8 and following sections for more details).

Electrochemical Data Acquisition. The individually addressable nanogap transducers in an array chip were connected to a custom-made printed circuit board (PCB) through contact pads on the chip and electrical contact pins that were mounted on the socket body (Figure S8). The reaction temperature was controlled by a Peltier thermoelectric cooling (TEC) device with a built-in thermocouple temperature sensor. The PCB was controlled by a LabVIEW program for cyclic voltammetry (CV) measurements. The measurement electronic system could detect subpicoampere currents with variable scan rates.

Chemical Abbreviations and Organic Synthesis. AP or pAP = *para*-aminophenol or 4-aminophenol; pAPP = *para*-aminophenyl monophosphate; pAPP$_3$ = *para*-aminophenyl triphosphates; each of the 4 letters (A, G, C, T) could mean a base, a nucleoside, a nucleotide, or a corresponding analog depending on the context, for example, A for deoxyadenosine, G for deoxyguanosine, C for deoxycytidine, T for thymidine, N for any of the 4 letters A, G, C, or T; AP-dN4P = δ-(*p*-aminophenyl) 2′-deoxyribonucleoside tetraphosphates; N$_3$-dNTPαS = 3′-*O*-azidomethyl, -2′-deoxyribonucleoside α-thiol-triphosphates. Methods for AP-dN4P synthesis and N$_3$-dNTPαS synthesis are outlined in Supporting Information according to published methods.[36−39]

Biochemical Buffers and Solutions. In this study, all enzymes were purchased from New England BioLabs and chemical reagents were from Sigma-Aldrich and Thermo-Fisher unless otherwise specified. 1 × B5 buffer included 10 mM Tris-HCl (pH 8.0), 50 mM NaCl, 5 mM $MgCl_2$ and 1 mM DTT (Dithiothreitol). Exo III reaction buffer included 1 × B5 buffer and 0.125 U/μL Exonuclease III. TEST reaction buffer with normal amount of enzymes (1×) included 0.15 U/μL Klenow exo$^-$ (K), 0.5 U/μL Exonuclease III (E), 0.15 U/μL CIAP (calf intestine alkaline phosphatase), 200 μM AP-dN4P, and 1 × B5 buffer. For on-chip-reactions, the reaction conditions were 1 × K, 2 × E, and 1 × C. FILL reaction buffer included 20 mM Tri-HCl (pH 8.0), 10 mM NH_4Cl, 5 mM $MgCl_2$, 10 mM KCl, 5 mM $MnCl_2$, 15 mM Na-Citrate, 0.5% Tween-20, 200 μM N$_3$-dNTPαS, and 0.2 U/μL therminator III. Wash buffer for DNA-magnetic beads included 10 mM EDTA (ethylenediaminetetraacetic acid), 0.1 μg/μL BSA (bovine serum albumin), 0.1% Tween 20, 20 mM Tris-HCl (pH 7.5), and 1 M NaCl. TCEP solution included 25 mM TCEP [Tris (2-carboxyethyl) phosphine], 100 mM Tris-HCl (pH 10.0), 100 mM NaCl, 1 mM EDTA, 20 mM DTT and 0.1% Tween 20. 1 × T3 buffer included 20 mM Tris-HCl (pH 8.0), 1 M NaCl, 0.1 μg/μL BSA, 10 mM EDTA, and 0.1% Tween-20. DNA-beads preparation and immobilization on nanogap transducer array chip surface are described in Supporting Information.

FILL Reaction with N$_3$-dNTPαS. The FILL reaction served two purposes: (1) extending each priming end with a single base and (2) rendering priming termini nuclease resistant. FILL reactions were performed with DNA template molecules attached to magnetic beads that were either in suspension or attached on a chip surface. The four bifunctional nucleoside triphosphates (N$_3$-dNTPαS) were used for the reactions, each of which had a reversible terminator at the 3′-end and an α-thiol-phosphate at the corresponding 5′-end. The procedure typically included the following steps: (i) conditioning the DNA-beads with B5 buffer; (ii) prior to the TEST reaction, removing non-α-thiol nucleotides from the 3′-ends by performing Exo III digestion for 10 min at 37 °C, followed by 1 × B5 buffer wash; (iii) extending the priming ends with 200 μM N$_3$-dNTPαS with therminator III (0.3 U/μL) at 68 °C for 15 min, followed by washing with 1 × T3 buffer and then 1 × B5 buffer, both for 5 min at 50 °C; (iv) removing the reversible terminator by TCEP treatment at 68 °C for 10 min, followed by 1 × B5 buffer wash; then (v) proceeding to the next TEST reaction if mini-sequencing was being performed.

TEST Reaction with AP-dN4P. TEST reactions were performed in four sequential reactions, each with one of the four AP-dN4Ps and an enzyme cocktail containing exo$^-$ Klenow DNA polymerase of the *E. coli* DNA polymerase I, exonuclease III, and phosphatase (all from New England BioLabs). When TEST reactions were performed in test tubes with DNA-beads in suspension, aliquots of reaction products were retrieved from a test tube in 10 min or at desired time intervals after separating the DNA-magnetic beads. Redox cycling signals of pAP from different sample aliquots were measured with nanogap devices in a flowcell. When TEST reactions were performed in a flowcell where DNA-beads were immobilized, redox cycling signals could be measured any time during the reactions. Typically, data were acquired at the intervals of 2 to 5 min for a total time of 20 min or up to 40 min. For every new reagent exchange, it typically took about 2 min for the reaction system to be stabilized. A typical TEST procedure included the following steps: (i) filling the flowcell chamber with a TEST reaction mixture containing one of the four AP-dN4Ps (note that the flowcell chamber was preheated to 39 °C or a desired temperature, measured at the heating block (not in the chamber) and thus actual temperature experienced by the sample was 1−2 °C lower); (ii) recording CV responses at desired time intervals; (iii) repeating the above procedure for the remaining 3 nucleotide analogs; (iv) proceeding to next FILL reaction if mini-sequencing was being performed.

Electrochemical Measurement and Kinetics Data Analysis. CV curves were typically obtained by sweeping the voltage at the bottom (or top) electrode from 0 to 0.8 V for an aqueous sample. CV curves were obtained from buffer (1 × B5) to monitor system baseline stability. For off-chip reactions, a CV curve was taken 2 min after the

DOI: 10.1021/acssensors.8b00500
ACS Sens. XXXX, XXX, XXX−XXX

sample was introduced into a flowcell. For on-chip TEST reactions, CV curves were measured at given temperature for every 2 to 5 min without disturbing the reactions inside the flowcell chamber. For each CV curve, the redox signal (RS) was determined by subtracting intra baseline (IB) value from absolute reading (AR) at a given voltage (Figure S6): RS = AR − IB. IB was the electrochemical current value determined by linearly extrapolating from the early linear portion of the CV curve that was from 0 V to the inflection point (Figure S6). Typically, the IB values could be the same among a set of TEST reactions under the same conditions, but we noticed that IB was more reliable for use as the baseline for its own CV curve than the value from the CV curve of the blank buffer (1 × B5) because the presence of additional biochemical reagents in a solution could slightly increase the baseline compared to plain buffer. Using either approach, the reported trends in the experimental results were the same. The reaction kinetics were evaluated according to reaction rate laws,[40,41] and details are provided in Supporting Information.

Mini-Sequencing Method. See Supporting Information for details. Briefly, to determine if a newly incorporated nucleotide base was correctly paired or mispaired, we first normalized pAP production rates of a given nucleotide analog across all base positions on the same DNA template in the same reaction setup. Once normalized reaction rates of all 4 nucleotide analogs for every base position of a DNA template had been calculated, the interrogated base could be determined by the highest normalized reaction rate ratio value among the 4 different nucleotide analogs for the given position.

■ ASSOCIATED CONTENT

Supporting Information

The Supporting Information is available free of charge on the ACS Publications website at DOI: 10.1021/acssensors.8b00500.

Supplementary methods, biochemistry methods, electrochemical kinetic data analysis, mini-sequencing method, including figures and data (PDF)

■ AUTHOR INFORMATION

Corresponding Author

*E-mail: xing.su@intel.com or xingsu516@gmail.com.

ORCID

Xing Su: 0000-0002-4135-453X

Grace M. Credo: 0000-0003-2493-4257

Present Addresses

[†]D.J.L.: Gilead Sciences, 333 Lakeside Dr., Foster City, CA 94404, USA.

[‡]J.S.D.: Applied Scientific Instrumentation, 29391 W Enid Rd., Eugene, OR 97402, USA.

[§]H.L.: Complete Genomics Inc., 2904 Orchard Pkwy, San Jose, CA 95134.

[∥]D.A.H.: Univ. of California, San Diego, 9500 Gilman Dr. La Jolla, CA 92093, USA.

[⊥]M.V.: LabCyte Inc., 170 Rose Orchard Way, San Jose, CA 95134, USA.

Author Contributions

[#]N.T., G.M.C., K.W., and O.H.E. contributed equally. X.S. and K.W. conceived TEST & FILL concept; X.S. and D.J.L. conceived redox-genic concept; J.S.D. and O.H.E. were responsible for driving the development of the redox cycling approach; O.H.E. and N.T. designed and fabricated nanogap devices; J.S.D. and D.A.H. developed the modular electronic measurement systems; N.T., G.M.C., H.L., and X.S. conceived and validated the nanogap coating concept; D.A.H. and X.S. developed the measurement flow cell; D.J.L., H.L., G.M.C., and X.S. developed redox chemistry; K.W., X.S., and G.M.C. performed enzyme assays; M.V., X.S., and O.H.E. performed project management; X.S., N.T., G.M.C., D.A.H., and K.W. analyzed key data, made main conclusions, and prepared the manuscript.

Notes

The authors declare no competing financial interest.

■ ACKNOWLEDGMENTS

The work described in this paper was conducted at and supported by an internal research program at Intel Corporation. We thank Samuel S. Tan, Ruiming Zou, Konstantin Kisly, and John Lee for supporting organic synthesis, Qing Yang, Hsiao C. Lim, Mun Hua Tan, and Calvin Wong for supporting bioassays, and William van Trump and Liming Wang for assistance with electrochemistry and instrumentation.

■ REFERENCES

(1) Acker, M. G.; Auld, D. S. Considerations for the Design and Reporting of Enzyme Assays in High-throughput Screening Applications. *Perspectives in Science* **2014**, *1*, 56−73.

(2) Léger, C.; Bertrand, P. Direct Electrochemistry of Redox Enzymes as a Tool for Mechanistic Studies. *Chem. Rev.* **2008**, *108*, 2379−2438.

(3) Ullrich, S. J.; Hellmich, U. A.; Ullrich, S.; Glaubitz, C. Interfacial Enzyme Kinetics of a Membrane Bound Kinase Analyzed by Real-time MAS-NMR. *Nat. Chem. Biol.* **2011**, *7*, 263−270.

(4) Eriksson, J.; Langel, Ü. Quantitative Microplate Assay for Real-time Nuclease Kinetics. *PLoS One* **2016**, *11*, e0154099.

(5) Yu, C.; Sun, Q.; Zhou, H. Enzymatic Screening and Diagnosis of Lysosomal Storage Diseases. *N. Am. J. Med. Sci. (Boston).* **2013**, *6*, 186−193.

(6) Michal, G.; Schomburg, D., Ed. *Biochemical Pathways: An Atlas of Biochemistry and Molecular Biology*; Wiley: New York, 1999.

(7) Heinonen, J. K. *Biological Role of Inorganic Pyrophosphate*; Springer Science & Business Media, 2001.

(8) Pourmand, N.; Karhanek, M.; Persson, H. H.; Webb, C. D.; Lee, T. H.; Zahradníková, A.; Davis, R. W. Direct Electrical Detection of DNA Synthesis. *Proc. Natl. Acad. Sci. U. S. A.* **2006**, *103*, 6466−6470.

(9) Rothberg, J. M.; Hinz, W.; Rearick, T. M.; Schultz, J.; Mileski, W.; Davey, M.; Leamon, J. H.; Johnson, K.; Milgrew, M. J.; Edwards, M.; Hoon, J.; et al. An Integrated Semiconductor Device Enabling Non-optical Genome Sequencing. *Nature* **2011**, *475*, 348−352.

(10) Liu, D. J.; Credo, G. M.; Su, X.; Wu, K.; Lim, H. C.; Elibol, O. H.; Bashir, R.; Varma, M. Surface immobilizable chelator for label-free electrical detection of pyrophosphate. *Chem. Commun.* **2011**, *47*, 8310−8312.

(11) Credo, G. M.; Su, X.; Wu, K.; Elibol, O. H.; Liu, D. J.; Reddy, B.; Tsai, T.-W.; Dorvel, B. R.; Daniels, J. S.; Bashir, R.; Varma, M. Label-free electrical detection of pyrophosphate generated from DNA polymerase reactions on field-effect devices. *Analyst* **2012**, *137*, 1351−1362.

(12) Elibol, O. H.; Daniels, J. S.; Credo, G. M.; Su, X. Nanogap chemical and biochemical sensors. U. S. Patent 8,500,979, 2013.

(13) Zevenbergen, M. A.; Krapf, D.; Zuiddam, M. R.; Lemay, S. G. Mesoscopic Concentration Fluctuations in a Fluidic Nanocavity Detected by Redox Cycling. *Nano Lett.* **2007**, *7*, 384−388.

(14) Rassaei, L.; Mathwig, K.; Kang, S.; Heering, H. A.; Lemay, S. G. Integrated Biodetection in a Nanofluidic Device. *ACS Nano* **2014**, *8*, 8278−8284.

(15) Kätelhön, E.; Wolfrum, B. On-chip Redox Cycling Techniques for Electrochemical Detection. *Rev. Anal. Chem.* **2012**, *31*, 7−14.

(16) Zevenbergen, M. A.; Singh, P. S.; Goluch, E. D.; Wolfrum, B. L.; Lemay, S. G. Stochastic Sensing of Single Molecules in a Nanofluidic Electrochemical Device. *Nano Lett.* **2011**, *11*, 2881−2886.

DOI: 10.1021/acssensors.8b00500
ACS Sens. XXXX, XXX, XXX−XXX

(17) Elibol, O. H.; Akkaya, O. C.; Credo, G. M.; Daniels, J. S.; Tayebi, N. Diamond Electrode Nanogap Transducers. U. S. Patent 9,322,798, 2016.
(18) Majni, G.; Ottaviani, G.; Prudenziati, M. Interdiffusion of Thin Cr and Au Films Deposited on Silicon. *Thin Solid Films* **1976**, *38*, 15−19.
(19) May, P. W. Diamond Thin Films: A 21st-Century Material. *Philos. Trans. R. Soc., A* **2000**, *358*, 473−495.
(20) Hall, D. A.; Daniels, J. S.; Geuskens, B.; Tayebi, N.; Credo, G. M.; Liu, D. J.; Li, H.; Wu, K.; Su, X.; Varma, M.; Elibol, O. H. A Nanogap Transducer Array on 32nm CMOS for Electrochemical DNA Sequencing. Proceedings of IEEE ISSCC (International Solid-State Circuits Conference, January 31−February 4, San Francisco, CA), 2016.
(21) Tang, H. T.; Lunte, C. E.; Halsall, H. B.; Heineman, W. R. p-Aminophenyl Phosphate: an Improved Substrate for Electrochemical Enzyme Immunoassay. *Anal. Chim. Acta* **1988**, *214*, 187−195.
(22) Dwyer, D. J.; Cameron, S. D.; Gland, J. Surface Modification of Platinum by Titanium Dioxide Overlayers: A Case of Simple Site Blocking. *Surf. Sci.* **1985**, *159*, 430−442.
(23) Yang, Z.; Sismour, A. M.; Benner, S. A. Nucleoside Alpha-thiotriphosphates, Polymerases and the Exonuclease III Analysis of Oligonucleotides Containing Phosphorothioate Linkages. *Nucleic Acids Res.* **2007**, *35*, 3118−3127.
(24) Li, Z.; Bai, X.; Ruparel, H.; Kim, S.; Turro, N. J.; Ju, J. A Photocleavable Fluorescent Nucleotide for DNA Sequencing and Analysis. *Proc. Natl. Acad. Sci. U. S. A.* **2003**, *100*, 414−419.
(25) Joyce, C. M. How DNA Travels Between the Separate Polymerase and 3′-5′-exonuclease Sites of DNA Polymerase I (Klenow fragment). *J. Biol. Chem.* **1989**, *264*, 10858−10866.
(26) Mizrahi, V.; Benkovic, P. A.; Benkovic, S. J. Mechanism of the Idling-turnover Reaction of the Large (Klenow) Fragment of Escherichia coli DNA Polymerase I. *Proc. Natl. Acad. Sci. U. S. A.* **1986**, *83*, 231−235.
(27) Cox, B. G. *Modern Liquid Phase Kinetics*; Oxford University Press; 1994.
(28) Chappelet-Tordo, D.; Fosset, M.; Iwatsubo, M.; Gaché, C.; Lazdunski, M. Intestinal Alkaline Phosphatase. Catalytic Properties and Half of the Sites Reactivity. *Biochemistry* **1974**, *13*, 1788−1795.
(29) Pugliese, K. M.; Gul, O. T.; Choi, Y.; Olsen, T. J.; Sims, P. C.; Collins, P. G.; Weiss, G. A. Processive Incorporation of Deoxynucleoside Triphosphate Analogs by Single-molecule DNA Polymerase I (Klenow fragment) Nanocircuits. *J. Am. Chem. Soc.* **2015**, *137*, 9587−9594.
(30) Joyce, C. M.; Benkovic, S. J. DNA Polymerase Fidelity: Kinetics, Structure, and Checkpoints. *Biochemistry* **2004**, *43*, 14317−14324.
(31) Wang, Y.; Zhou, X. L.; Ruan, Z. R.; Liu, R. J.; Eriani, G.; Wang, E. D. A Human Disease-causing Point Mutation in Mitochondrial Threonyl-tRNA Synthetase Induces Both Structural and Functional Defects. *J. Biol. Chem.* **2016**, *291*, 6507−6520.
(32) Loeb, L. A.; Monnat, R. DNA Polymerases and Human Disease. *Nat. Rev. Genet.* **2008**, *9*, 594−604.
(33) Sagong, B.; Baek, J. I.; Oh, S. K.; Na, K. J.; Bae, J. W.; Choi, S. Y.; Jeong, J. Y.; Choi, J. Y.; Lee, S. H.; Lee, K. Y.; Kim, U. K. A Rapid Method for Simultaneous Screening of Multi-gene Mutations Associated with Hearing Loss in the Korean Population. *PLoS One* **2013**, *8*, e57237.
(34) De Clercq, E. Antiviral Drug Discovery and Development: Where Chemistry Meets with Biomedicine. *Antiviral Res.* **2005**, *67*, 56−75.
(35) Jordheim, L. P.; Durantel, D.; Zoulim, F.; Dumontet, C. Advances in the Development of Nucleoside and Nucleotide Analogues for Cancer and Viral Diseases. *Nat. Rev. Drug Discovery* **2013**, *12*, 447−464.
(36) Korlach, J.; Bibillo, A.; Wegener, J.; Peluso, P.; Pham, T. T.; Park, I.; Clark, S.; Otto, G. A.; Turner, S. W. Long, Processive Enzymatic DNA Synthesis Using 100% Dye-labeled Terminal Phosphate-linked Nucleotides. *Nucleosides, Nucleotides Nucleic Acids* **2008**, *27*, 1072−1082.
(37) Sims, P. A.; Greenleaf, W. J.; Duan, H.; Xie, X. S. Fluorogenic DNA Sequencing in PDMS Microreactors. *Nat. Methods* **2011**, *8*, 575−580.
(38) Guo, J.; Xu, N.; Li, Z.; Zhang, S.; Wu, J.; Kim, D. H.; Marma, M. S.; Meng, Q.; Cao, H.; Li, X.; Shi, S. Four-color DNA Sequencing with 3′-O-modified Nucleotide Reversible Terminators and Chemically Cleavable Fluorescent Dideoxynucleotides. *Proc. Natl. Acad. Sci. U. S. A.* **2008**, *105*, 9145−9150.
(39) Eckstein, F. Nucleoside Phosphorothioates. *Annu. Rev. Biochem.* **1985**, *54*, 367−402.
(40) Bergethon, P. R. *The Physical Basis of Biochemistry: the Foundations of Molecular Biophysics*; Springer Science & Business Media, 2013.
(41) Hindmarsh, K.; House, D. A. An Easily Demonstrated Zero-order Reaction in Solution. *J. Chem. Educ.* **1996**, *73*, 585.

DOI: 10.1021/acssensors.8b00500
ACS Sens. XXXX, XXX, XXX−XXX